Mathematical Framework for Predicting Solar Thermal Build-up of Spectrally Selective Coatings at the Earth's Surface

N. P. Lavery[†]

Materials Research Centre, University of Wales Swansea, Singleton Park, Swansea SA2 8PP, United Kingdom

27th July 2005

Abstract

A transient finite element thermal model is formulated valid for surface coatings on any substrate material and based on the continuum conduction equations with solar loading as a heat source. The model allows cooling to be applied at outer surfaces of the body, by natural convection and accounts for ambient radiative heat loss. Hemispherical spectral reflectivities are obtained for various polymer-based coatings on a steel substrate using spectrophotometers in the 0.1μm to 25μm wavelengths. A time-dependent solar irradiation energy source (black-body equivalent) is applied to an object with spectrally diffuse outer surfaces, and the incoming heat flux is split by a band approximation into reflected and absorbed energy and finally integrated over the complete spectrum to provide thermal source terms for the finite element model.

Results show that cyclic diurnal thermal build-up of temperature can be predicted for a body with different spectrally selective coatings. While the model exhibits the classic relationship for thermal build-up with colour, i.e. dark colours absorb more heat and

[†] Corresponding author, e-mail address: N.P.Lavery@swansea.ac.uk (Nicholas P. Lavery)

lighter colours remain cooler, it also shows that colours which appear similar can have very different thermal build-ups, depending on the infra-red reflectivity of the coating.

The general suitability of the finite element method to describe geometrically complex bodies coupled with additional parameters such as latitude, longitude and a variable ambient temperature can be used to simulate a variety of scenarios for a diverse number of applications.

Keywords – *Finite element heat transfer; spectrally selective coatings; solar loading;*

Nomenclature

A	Area of surfaces (m^2)	c_p	Specific heat capacity for metal or air (kJ/kg.K)
d	Solar declination (degrees)	G_0	Solar constant (1.395 kW/m^2)
$F_{0-\lambda T}$	Black body energy fraction (temperature T, wavelength λ)	h_r	Local hour angle of sun
k	Thermal conductivity for metal or air (W/m.K)	l	Latitude at Earth's surface (degrees)
q^{conv}	Energy lost by natural convection from surface (W)	q^{rad}	Energy lost by radiation from surface (W)
T_{sol}	Temperature of blackbody equivalent to radiation received from sun (K)	T_∞	Temperature of the surrounding ambient air (K)
T_S	Temperature at the surface (K)	T_f	Temperature in the thin film close to the surface (K)
t_a	Transmission coefficient for solar irradiation (0.81 clear day, 0.62 cloudy)	z	Zentith angle subtended by sun at object on Earth's surface
β	Volume coefficient of expansion, 1/K (Air)	ε_T	Total (low temperature) emissivity of surface
λ	Wavelength	μ	Dynamic viscosity air (kg/ms)
ρ	Density air or metal (kg/m^3)	$\rho_{\lambda_1-\lambda_2}$	Average hemispherical spectral reflectivity between wavelengths λ_1 and λ_2
σ	Stefan-Boltzmann constant	υ	Kinematic viscosity of air (m^2/s)

$\rho_\lambda(\lambda)$	Hemispherical spectral reflectivity	$\varepsilon_\lambda(\lambda)$	Hemispherical spectral emissivity
L	characteristic length, taken as 1 m	h	Heat transfer coefficient (W/m^2K)
Pr	Prandtl number	$\Pr = \frac{C_p \mu}{k}$	
Gr	Grashof number	$Gr = \frac{g\beta(T_s - T_\infty) * L^3}{\upsilon^2}$	
Ra	Rayleigh number	$Ra = Gr \Pr$	
Nu	Nusselt number	$Nu = \frac{hL}{k}$	

Introduction

Thermal modelling of solar loading in conjunction with convective and conductive heat transfer aspects continues to be of interest in a variety of applications ranging from buildings [1, 2], solar panels and collectors [3-6], environmental modelling [7, 8], to solar gains in oil pipelines [9] and military vehicles and objects [10].

Until recently, there were only a limited amount of possibilities that were available to the thermal engineer in terms of formulated paint coatings. With the new generation of spectrally selective paints and coatings, [11], specifically formulated to provide particular thermal characteristics which contradict intuitive associations of colour and temperature: dark colours no longer necessarily have to have the greatest thermal build-up. It may be that, in this sense, nature has already pre-empted man in achieving spectrally selective colouring. Chlorophyll accounts for the dark green colouring of plants, and even in direct sunlight on hot days, it will still feel cool. Although some of this coolness may be attributed to internal cooling systems, a look at the spectral distribution of reflectance of grass shows that it is highly reflecting in the infrared wavelengths.

The visible wavelength range accounts for 47% of the incident extraterrestrial solar radiation, and Ultra-Violet (UV) accounts for 7%. Colour is a property of the material manifested in the visible wavelength range, thus, there will always be a strong correlation

between colour and temperature. However, 46% of the incident radiation is in the Infra-Red (IR) range. This explains why it is possible to have materials with a high infrared reflectance and a dark colour (low visible reflectance) such as chlorophyll, which remain relatively cooler than other materials of the same visible colouring. In some applications, the inverse situation may be required, e.g. a light colour with maximum solar absorption.

The purpose of this work is to provide a mathematical framework for the thermal engineer connecting a standard finite element thermal model with spectral radiative heat transfer and a solar heat source at earth ground level. This is done in a practical manner to the extent that surface reflectance data for the material/coating can be directly imported from a spectrophotometer to give an idea of thermal build-up for a variety of environmental surroundings. These include the possibility of taking natural convection heat loss, forced convective wind cooling and a variety of locations on the Earth's surface. The general nature of the model formulation effectively means that the coatings in question can also encompass composite coatings with reflective substrates coated with a black spectrally selective paint, for which all the input data that is needed is the reflective spectrum of the coating and knowledge of basic material properties of the composite coating such as density, thermal conductivity and specific heat capacity.

1 THE GOVERNING EQUATIONS

1.1 Incident Solar Radiation

Solar incident radiation received by Earth at the outer atmosphere can be approximated to be the equivalent received from a black body emitter (the sun) at a temperature of Tsol=5800K, correct except in the lower ultraviolet (UV) range. This black-body

approximation can easily be extended to get equations which connect latitude and time of year, as shown in Figure 1, however, and as shown in Figure 2, the approximation does not capture the losses in the radiative flux intensity due to the various gas and water absorption bands in the atmosphere.

The total solar radiation incident on an imaginary surface just outside on the Earth's atmosphere is given by G_0 =1.395 kW/m2, and is known as the solar constant. The direct solar irradiation for an object at the Earth's surface is less than the solar constant and can be expressed as a fraction of it, by:

$$I_{sol} = G_0 \cos(z) t_a^{\sec(z)} \qquad \text{Eq 1}$$

Where t_a is a transmission coefficient for unit air mass (0.81 clear day, 0.62 cloudy), and z is the zenith angle, given by, [12, 13]:

$$\cos(z) = \sin(l)\sin(d) + \cos(l)\cos(d)\cos(h_r) \qquad \text{Eq 2}$$

Here, l is the latitude, d is the declination and h_r is the local hour angle. Diffuse sky radiation could also be taken into account to get a global incident solar radiation in Eq 1, but as this is generally substantially smaller than the direct radiation, it has temporarily ignored.

Declination lies in the range ±23.4° and can quite readily be obtained accurately to within 1% from the usual equation used in most textbooks [13, 14]:

$$d = 23.45 \sin\left(\frac{360}{365(284+n)}\right) \qquad \text{Eq 3}$$

Here n is the nth day of the year (Jan 1st is n=1). However, in this work, we have used the slightly more accurate version of this equation suggested by [15].

1.2 Spectral Energy Bands

Plank's equation for the emissive power of a black body is:

$$E_{\lambda b}(\lambda,T)=\frac{2\pi C_1}{\lambda^5\left(e^{C_2/\lambda T}-1\right)} \qquad \text{Eq 4}$$

T is temperature; lambda is the wavelength and C_1 and C_2 are constants, which can be found in [3], [4]. This equation can be integrated numerically to obtain the blackbody energy fraction in a particular wavelength band:

$$F_{0-\lambda T}=\frac{2\pi C_1}{\sigma T^4}\int_0^{\lambda}\frac{d\lambda}{\lambda^5\left(e^{C_2/\lambda T}-1\right)} \qquad \text{Eq 5}$$

Thermal energy is transmitted in the 0.1-100μm range. The reflectivity of some paints in the 0.3-2.5μm wavelength region is shown in Figure 3. The spectrum is made discrete by averaging over 0.1 intervals in the 0.1-1.0μm regions, 0.5 intervals in the 1.0-2.5μm region, and over the single 2.5-100μm regions. The total absorbed and reflected solar energy can now be obtained in terms of the flux per square metre by summing over all the wavelengths bands:

$$E_{reflected}=\frac{q_{ref}}{A}=\sum_{\lambda_1-\lambda_2=1}^{nr}\left(\frac{\rho_{\lambda_1-\lambda_2}}{100}\right)\times I_{sol}\times F_{\lambda_1-\lambda_2} \qquad \text{Eq 6}$$

$$E_{absorbed}=\frac{q_{abs}}{A}=\sum_{\lambda_1-\lambda_2=1}^{nr}\left(1-\frac{\rho_{\lambda_1-\lambda_2}}{100}\right)\times I_{sol}\times F_{\lambda_1-\lambda_2} \qquad \text{Eq 7}$$

In equations 6 and 7, nr is the number of band regions. Using the black body spectral distribution for solar irradiation represents the maximum radiation possible. In actual fact, transmittance factors such as molecular scattering, aerosol attenuation, water vapour absorption, ozone absorption, and uniformly mixed gas absorption should be accounted

for, and there exist columnar-based approximation models which can actually take into account these absorption bands, [16], and would provide better solar irradiation values.

However, these factors all act to reduce the irradiation, thus the blackbody irradiation used in the current model remains as the worst- or best-case scenario depending on the application. Some of these transmittance factors can be lumped into the transmission coefficient, as described in the previous section.

For the purpose of clarity, the thermal electromagnetic spectrum will henceforth be classified into the Ultraviolet (UV) spectrum 0.28-0.38μm, visible spectrum 0.38-0.74μm, Near Infrared (IR) spectrum 0.74-1.4μm, Medium IR spectrum 1.4-15μm, and Far IR spectrum 15-100μm.

1.3 Natural Convective Energy Loss

To describe the natural convection, a skin temperature needs to be defines as being the film temperature next to the surface that is loosing heat to convection. Then a suitable approximation is that the skin temperature is given by:

$$T_f = \frac{T_\infty + T_S}{2} \qquad \text{Eq 8}$$

Where T_∞ is the ambient temperature and T_s is the temperature of the surface at which the convection is taking place. For air at atmospheric temperature, values of the volume coefficient of expansion, β, can be obtained from the ideal gas law, as $\beta = 1/T_f$. and other properties such as the kinematic viscosity, ν, the thermal conductivity, *k*, and the Prandtl number, Pr, can be obtained from Table 1.

Once the properties have been established for a surface at a given temperature, the Rayleigh number, Ra, is calculated from:

$$Ra = \frac{g\beta(T_s - T_\infty) * L^3 * \mathrm{Pr}}{\upsilon^2} \qquad \text{Eq 9}$$

Where, in this case, the characteristic length is taken as one metre, i.e. L=1. The Rayleigh number can then be used to obtain the Nusselt number, and the form of this equation is different depending on whether the surface is vertical or horizontal:

Vertical surfaces [17] $Nu^{\frac{1}{2}} = 0.825 + \dfrac{(0.387 * Ra^{0.1666})}{\left(1 + \left(\dfrac{0.492}{\mathrm{Pr}}\right)^{0.5625}\right)^{0.2963}}$ (a) Eq 10

Horizontal surfaces [18] $Nu = C_A (Ra)^{C_B}$ (b)

The constants C_A and C_B are determined by the Raleigh number, i.e. if 10^5<Ra<$2x10^7$, then C_A =0.54 and C_B =0.25, else if $2x10^7$<Ra<$3x10^{10}$, then C_A =0.14 and C_B =0.33. For all of the cases looked at in this work, the Raleigh number fell within the latter range. Finally, the heat transfer coefficient for the system, h (W/m^{2}K) can be obtained from:

$$h = \frac{kNu}{L} \qquad \text{Eq 11}$$

Where, a length scale of L=1m has been used. Using this heat transfer coefficient, the energy flux loss can then be obtained from:

$$\frac{q^{conv}}{A} = h(T_\infty - T_S) \qquad \text{Eq 12}$$

For natural convection from vertical surfaces with temperatures up to a 150°C higher than ambient, this coefficient is of the order of 5 to 25 W/m^2, see [13, 17]. It should be

noted that the ambient temperature itself is also described by a modified periodic equation with respect to the daily local hour that accommodates maximum and minimum daily temperatures. Typical variations of the ambient temperature are given in the examples in the results section.

1.4 Radiative Energy Loss

At the same time that the surface is being heated up, it is also re-radiating to the surroundings, and this energy relationship uses the Stefan-Boltzmann equation:

$$\frac{q^{rad}}{A} = \varepsilon_T \sigma \left(T_\infty{}^4 - T_S^4 \right) \qquad \text{Eq 13}$$

Where, ε_T , is the total hemispherical low temperature emissivity, and sigma is the Stefan-Boltzmann constant. For temperatures under 150°C, less than 0.1% of the total radiation leaving the body is in the 0 to 2.5μm wavelength range, thus, epsilon also represents the total average emissivity in the mid and far IR range. According to [17] and [19], values in the order of 0.9-0.95 are appropriate.

2 GOVERNING EQUATIONS

The two-dimensional time-dependent heat transfer due to conduction with radiative flux and convective boundary conditions can be written as:

$$\rho c_p \frac{\partial T}{\partial t} - k\left(\frac{\partial^2 T}{\partial x^2} + \frac{\partial^2 T}{\partial y^2} \right) = Q \qquad \text{Eq 14}$$

Where T is temperature, t is time, ρ is the density, c_p is the specific heat capacity and k is the thermal conductivity. The term Q is the net heat flux at the boundaries from

convection and radiation and is given by $Q = q^{conv} + q^{rad}$, where q^{conv} is given by equation 12 and q^{rad} is given by equation 13. Equation 14 is subject to the initial conditions:

$$T(x, y, t) = T_\infty \quad \text{at} \quad t = 0 \qquad \text{Eq 15}$$

Radiated, convected and absorbed energy flux contributions on the right hand side of the energy equations can be applied as surface boundary conditions in the finite element method.

2.1 Finite Element Solution

The Galerkin Finite element method, [20], with four nodded quadrilateral elements was used on equation 14, which results in a system of matrix equations of the form:

$$\underline{\underline{\mathbf{M}}} \left(\frac{\mathbf{T}^{n+1} - \mathbf{T}^n}{\Delta t} \right) + \underline{\underline{\mathbf{K}}} \mathbf{T}^{n+1} = \int_\Gamma \mathbf{q}_r^{rad}(\mathbf{T}^n) d\Gamma + \int_\Gamma \mathbf{q}^{conv} d\Gamma \qquad \text{(a)}$$

Eq 16

$$\begin{aligned} \mathbf{q}_r^{rad} &= \sigma \varepsilon_T \left(\hat{T}^n \right)^3 \mathbf{T}_r \\ \mathbf{T}_{r+1} &= \lambda \mathbf{T}_r + (1-\lambda) \mathbf{T}^{n+1} \qquad \text{(b)} \\ \mathbf{q}_{r+1}^{rad} &= \lambda \mathbf{q}_r^{rad} + (1-\lambda) \mathbf{q}_{r-1}^{rad} \end{aligned}$$

The coefficients of the mass, $\underline{\underline{\mathbf{M}}}$, and stiffness $\underline{\underline{\mathbf{K}}}$ matrices in equation 16 (a) can be found in [20]. An implicit time stepping scheme is used which is unconditionally stable, thus there were no problems in obtaining convergence for the time step of 3600 s (1 hour) and a spatial division of $\Delta x = \Delta y = 0.0166\,m$ as used in the test case problems examined. Prior to running cases with radiation, convection and solar loading boundary conditions, the finite element solution of the thermal conductivity equation was tested for a single

material with fixed temperatures at the left and right boundaries, and insulated top and bottom boundaries. The results were compared to the analytical solution, and only small deviations were found to occur from the analytical results, namely in terms of spatial and temporal convergence.

It should be noted that the radiative surface boundary condition introduces a non-linear aspect into the equations which has been linearised and treated iteratively at each time step using a relaxation parameter $\lambda = 0.5$. Typically about 10 non-linear iterations were required per time step so that the radiative flux converged to a tolerance of 10^{-2}. In equation 16(b), the $\left(\hat{T}^{n}\right)^{3}$ term represents a linearization of the Stefan-Boltzmann equation for radiative heat loss.

3 PAINT REFLECTIVITY DATA

Spectral reflectivity was obtained for 13 samples provided by CORUS of an industrially applied polymer using a Perkin-Elmer UV/VIS/NIR Lambda 9 and FT-IR Spectrum-1 spectrophotometer, by integrating over all angles of the hemisphere. Each sample was cut to 2.5cmx3.8cm, and the average coating was 220μm thick based on a substrate of 0.6 mm steel.

The samples were labelled according to their colour as: dark Blue (01), dark red (02), grey (03), green (04), light red (05), light blue (06), grey blue (07), beige-cream (08), ochre (09), white (10), yellow (11), brown (12), and black (13), and spectral reflectivity (%) data on the Lambda 9 in the visible range is shown in Figure 3. Note that peaks of reflectivity correspond with our perception of colours, as would be expected, i.e. dark colours have a lower reflectivity, and dark blue, for example, peaks in the blue region of

the spectrum (i.e. between 0.43 and 0.5μm), thus giving it the blue colour. Figure 4 shows the same data for the complete ultra-violet (UV), visible (VIS) and near-infrared (NIR) ranges as obtained with the Lambda 9.

Spectral reflectivity data obtained using the FT-IR for the Far Infra-red spectrum is shown in Figure 5. The data measured on this machine was highly prone to the positioning of the sample in the cup, and an average of approximately four readings per sample was used. However, in this range, the mid- to far- IR range, there was no longer any clear correlation between the reflectivity and the colour. In fact, white was found to be less reflective.

For the sampled coloured paints, various high absorption bands were seen to occur at similar locations in the spectrum in the FT-IR data, and are thought to be naturally occurring overtone bands (CH/CC/Polyester/Carbons/etc), and there is a particularly distinctive absorption band which can be seen in the 1.7μm range.

All spectral reflectivity data for the coatings were lumped into 13 distinct bands in the 0.3μm to 22μm ranges for use in the model via equations 6 and 7. The number of bands used was simply a way of reducing the data to a manageable size, and could easily be increased if greater accuracy was required.

The spectral reflectivity for nickel black 01/82, also generally known as 3M black paint, was obtained from [21], as it matched the spectral range being considered here. The constitutive base and substrate for this black is different to those of the other colours, as this colour is not supplied for this particular product range. While the high absorption of black coatings can be strongly driven by chemical composition, this may be seen as an

unfair comparison, however most black paints have reflectivity values significantly lower than 10% and do vary greatly over the range of spectra being considered here.

Finally, the reflectivity spectra for an ideal reflecting black pigment and a green leaf, as suggested by [11].

4 RESULTS

The geometry that was considered is shown in Figure 6 (not to scale) consists of a 1mx1m metal container coated with a selected paint and enclosing an air pocket. The paint was taken to have a small thickness (0.1 microns) with respect to the thickness of the metal (0.3 m). The simulation results presented here do not intend to accurately reproduce the environmental conditions at a given time and location, but rather to demonstrate the validity of the trends being predicted by the model, however it is possible to obtain data for solar irradiation, wind and ambient temperature at specific locations, and this will form the basis of future work. Thermo-physical temperature dependent properties for the air outside the container are listed at various temperatures in Table 1. The properties for the air inside the container, as well as for the steel walls were not allowed to vary with temperature, and are given in

Table **2**. The boundary conditions used are summarised in Table 3.

4.1 Case 1 – summer in Cairo, Egypt

The model parameters for this case were taken as: Latitude 30°N; Start analysis date 16 July at 00:00; End analysis date 19 July at 23:00; Minimum daily temperature 21.7°C at 06:00; Maximum daily temperature 34.4°C at 13:00 (Data obtained from the World Meteorological Organisation). The transmission coefficient for unit air mass was taken as

0.81 (a clear day), and diurnal variations of incident solar energy, absorbed energy, energy losses by convection and radiation are shown in figure 7. The maximum solar flux for this location and date was 1110.38 (W/m^2). The thermal build-up (maximum temperature of the paint/metal) for all paints during the three-day cycle is shown in figure 8, together with the ambient temperature. These are also shown in the 24 hour cycle in figure 9. The thermal build-up of a coating with equivalent spectral reflectance of green-leaf is compared to that for black, white and green, as well as using reflectance spectra for two hypothetical coatings: a) a black with ideal IR-reflectance and b) a green leaf, as obtained from [11].

As can be seen from figure 9, the thermal build-up of an ideal IR-reflector is 27% lower than that of black, and as there is no absorption in the IR range, this means that almost all the 13°C is due to the IR absorption bands. The thermal leaf-green is also 7% lower than the green paint, suggesting that there may be some potential of reducing the thermal build-up from both these paints by some amount. These should all be compared to the beige-cream paint which is a relatively light looking colour, but which has a relatively large thermal build-up when compared to green. Thus, within a small margin, it is possible to have darker colours which have a lower thermal build-up than visibly light colours.

The effects of varying the low temperature total emissivity parameter ε_T for the radiative loss boundary condition is shown as a function of maximum temperature in Figure 11, and as a function of the total energy lost by convection and radiation in Figure 12. Although the radiated heat lost to the environment is substantial, the effect of the emissivity parameter in the allowable ranges (0.7 to 0.99) was found to be small.

4.2 Case 2 – winter in Swansea, United Kingdom

The following parameters for this case: Latitude 52°N; Start analysis date 12 March at 00:00; End analysis date 16 March at 23:00; Minimum daily temperature 3°C at 06:00; Maximum daily temperature 9.7°C at 13:00 (Data obtained from the World Meteorological Organisation). The transmission coefficient for unit air mass was again taken as 0.81 (a clear day). The maximum solar flux for this location and date was 552.10 (W/m^2). The predicted thermal build-up for black and white paints for this case are compared to those in the previous case (Cairo) in figure 13.

5 FUTURE WORK

In the current work, solar loading is provided by treating the sun as a point source, thus not requiring direct calculation of any view factors, however, this could be taken a step further as in [24], where a disk is used to model the solar source. Indeed, work has already started in including the solar modelling described in this paper into an existing three-dimensional heat transfer model, [25-28], which uses Monte-Carlo and Hemi-cube algorithms to calculate view factors for surface-to-surface radiative heat transfer. This model can also include internal heat sources (such as engines) and be coupled to results emanating from CFD, and has a variety of applications to fixed and rotary wing aircraft in flight, as well as when stationary on the runway.

6 CONCLUSIONS

A solar loading, transient finite element thermal model has been presented which is valid for spectrally diffuse surface coatings on any substrate material and based on the continuum conduction equations.

Results have shown that cyclic diurnal thermal build-ups of temperature can be predicted for a body with different spectrally selective coatings. The model exhibits the classic relationship for thermal build-up with colour, i.e. dark colours absorb more heat and lighter colours remain cooler, but it also shows that colours which appear similar in the visible spectrum can have substantially different thermal build-up, depending on the reflectivity spectra in the infra-red range.

The general suitability of the finite element method to describe geometrically complex bodies coupled with additional parameters such as latitude, longitude and a variable ambient temperature can be used to simulate a variety of scenarios for a diverse number of applications.

7 ACKNOWLEDGEMENTS

The author would like to thank CORUS for the samples of paint provided.

8 REFERENCES

[1] A. K. Athienitis, M. Chandrashekar, and H. F. Sullivan, "Modelling and Analysis of Thermal Networks Through Subnetworks for Multizone Passive Solar Buildings," *Applied Mathematical Modelling*, vol. 9, pp. 109:116, 1985.

[2] F. Haghighat, "Thermal Behaviour of Buildings under Random Conditions," *Applied Mathematical Modelling*, vol. 11, pp. 349:356, 1987.

[3] J. P. Forsstrom and P. D. Lund, "Optimization of Operating Strategies in a Community Solar Heating System," *Applied Mathematical Modelling*, vol. 9, pp. 117:124, 1985.

[4] M. F. El-Refaie and M. A. Hashish, "Temperature Distributions in Flat-Plate Collector Under Actual Unsteady Insolation," *Applied Mathematical Modelling*, vol. 4, pp. 181:186, 1980.

[5] L. Cauli and D. Salimbeni, "A Control Method for Speeding Up Response of a Heating Plant with Solar-assisted Energy Recovery," *Applied Mathematical Modelling*, vol. 15, pp. 73:81, 1991.

[6] R. Patera and H. Robertson, "Green's Function Solution of the Time-dependent Solar Collector Problem," *Applied Mathematical Modelling*, vol. 8, pp. 365:369, 1984.

[7] B. Henderson-Sellers, "Sensitivity of Thermal Stratification Models to Changing Boundary Conditions," *Applied Mathematical Modelling*, vol. 12, pp. 31:43, 1988.

[8] G. Wang and M. Ostoja-Starzewski, "A Numerical Study of Plume Dispersion Motivated by a Mesoscale Atmospheric Flow over a Complex Terrain," *Applied Mathematical Modelling*, vol. 28, pp. 957:981, 2004.

[9] M. Murat Tunc, F. Taner Ozkaynak, and A. Souza, "Evaluation of Pressure Levels in Pipelines due to Solar Heat Gains," *Applied Mathematical Modelling*, vol. 9, pp. 16:20, 1985.

[10] G. Gimmestad, A. Millman, S. Lee, and S. Guitar, "The Diurnal Temperature Variations of an Object in an Outdoor Environment," *Applied Mathematical Modelling*, vol. 6, pp. 410:414, 1982.

[11] G. Burkhart, T. Detrie, and D. Swiler, "When Black is White," in *Paint and Coatings Industry Magazine*, 2000.

[12] L. Imre and L. Kiss, "Transient Thermal Performances of Composite Devices," in *Numerical Methods in Heat Transfer*, vol. II, R. H. Lewis, K. Morgan, and B. A. Schrefler, Eds., 1983, pp. 395:446.

[13] W. Grey and R. Muller, *Engineering Calculations in Radiative Heat Transfer*, vol. 13: Pergamon Press, 1974.

[14] G. G. Roy, M. Rodrigo, and W. King, "A note on solar declination and the equation of time," *Architectural Science Review*, vol. 32, pp. 43:51, 1989.

[15] B. Bourges, "Improvement in Solar Declination Computation," *Solar Energy*, vol. 35, pp. 367:369, 1985

[16] R. E. Bird, "A simple Spectral Model for Direct Normal and Diffuse Horizontal Irradiance," *Solar Energy*, vol. 32, pp. 461:471, 1984.

[17] J. P. Holman, *Heat Transfer*, 7th ed: McGraw-Hill Press, 1992.

[18] J. Welty, *Engineering Heat Transfer*: John Wiley & Sons, 1974.

[19] R. Siegel and J. Howell, *Thermal Radiation Heat Transfer*, 4 ed: Taylor and Francis, 2002.

[20] I. Smith and D. Griffiths, *Programming the Finite Element Method*, 3rd ed: Wiley, 1998.

[21] D. B. Betts, F. J. J. Clarke, L. J. Cox, and J. A. Larkin, "Infrared reflection properties of five types of black coating for radiometric detectors," *J. Phys. E: Sci. Instrum.*, vol. 18, 1985.

[22] "Standard Test Method D4803-97: Predicting Heat Build-up in PVC on Building Products," in *Annual Book of ASTM Standards*, vol. 08:04, 2001.

[23] M. D. Blue and S. Perkowitz, "Space-exposure effects on optical-baffle coatings at far-infrared wavelengths," *APPLIED OPTICS*, vol. 31, pp. 4305:4309, 1992

[24] S. Sugden, "View Factor for Inclined Plane with Gaussian Source," *Applied Mathematical Modelling*, vol. 28, pp. 1063:1082, 2004.

[25] N. Lavery , S. Brown , J. Spittle , L. Hayward , and S. Rooks "Finite Element Radiative and Conductive Module for use with PHOENICS," presented at 8th International PHOENICS User Conference, Luxembourg, 2000.

[26] N. Lavery, S. Brown, J. Spittle, S. Rooks, L. Hayward, and A. G. Smith, "A Coupled CFD-Thermal Solver prediction system for detailed platform IR prediction," presented at 11th Annual Ground Target Modelling & Validation Conference, Chicago, Michigan, USA, 2000.

[27] N. Lavery, S. Brown, J. Spittle, S. Rooks, L. Hayward, and A. G. Smith, "Improved modelling capabilities of PHARO: a coupled CFD-Thermal solver for detailed platform IR prediction," presented at 12th Annual Ground Target Modelling & Validation Conference, Chicago, Michigan, USA, 2001.

[28] N. Lavery , M. Vujicic , and S. Brown "Thermal Experimental Investigation of Radiative Heat Transfer for the Validation of Radiation Models," presented at Twelfth International Conference on Computational Methods and Experimental Measurements, Malta, 2005.

Table 1 – Thermally dependent properties of air at atmospheric pressure, from [17]

Temperature K	β / K	ν $m^2/s \times 10^6$	k W/mK	*Pr*
200	0.0050	11.31	0.02227	0.722
250	0.0040	15.69	0.02624	0.708
350	0.0030	20.76	0.03003	0.697
400	0.0025	25.90	0.03365	0.689

Table 2 – Non-thermally dependent material properties used for the steel and air, from [17]

	C_p $(kJ/kg.K)$	ρ (kg/m^3)	k W/mK
Steel (Carbon)	0.473	7800	43
Air (200-400K)	1.0	1.0	0.03

Table 3 – Boundary conditions used for test problem (see **Figure 6**)

Boundary condition	*Top Wall*	*Bottom Wall*	*Left Wall*	*Right Wall*
Solar radiation	Y	Insulated	Y	Y
Convective heat loss	Y (Eq. 10 b)	Insulated	Y (Eq. 10 a)	Y (Eq. 10 a)
Radiative heat loss	Y (Eq. 13)	Insulated	Y (Eq. 13)	Y (Eq. 13)

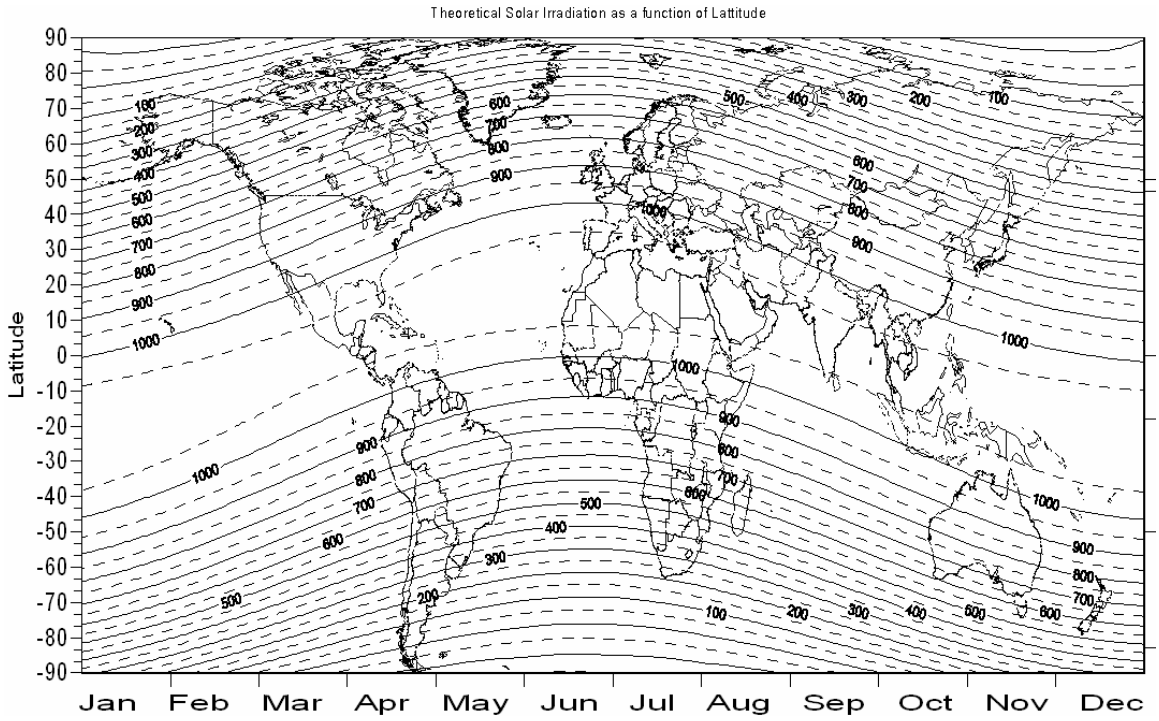

Figure 1 – Incident solar radiation (direct solar irradiation) as a function of latitude and month of the year given by equations 1-3

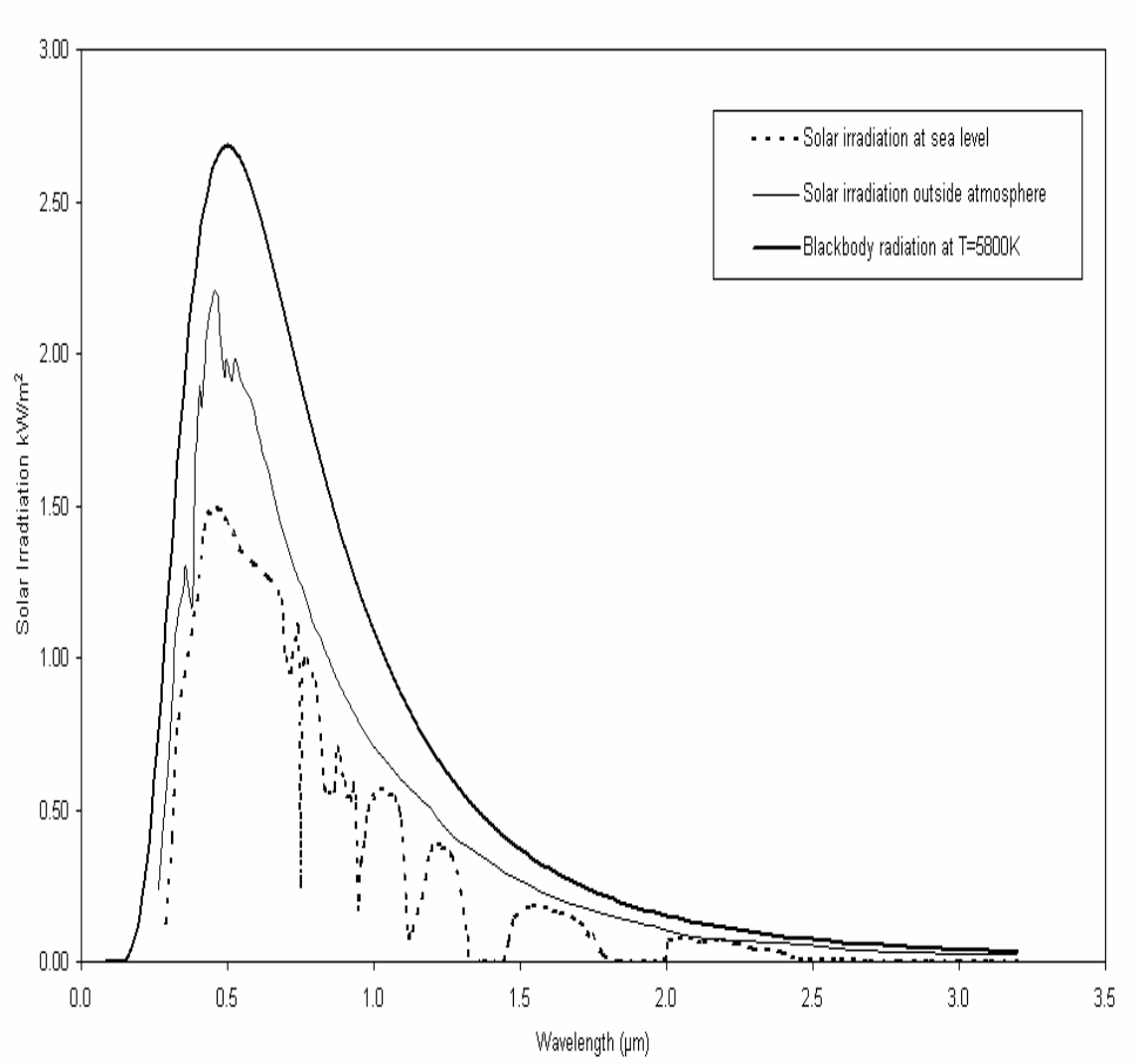

Figure 2 – Solar irradiation for a black-body at T=5800K and compared to data from [13]

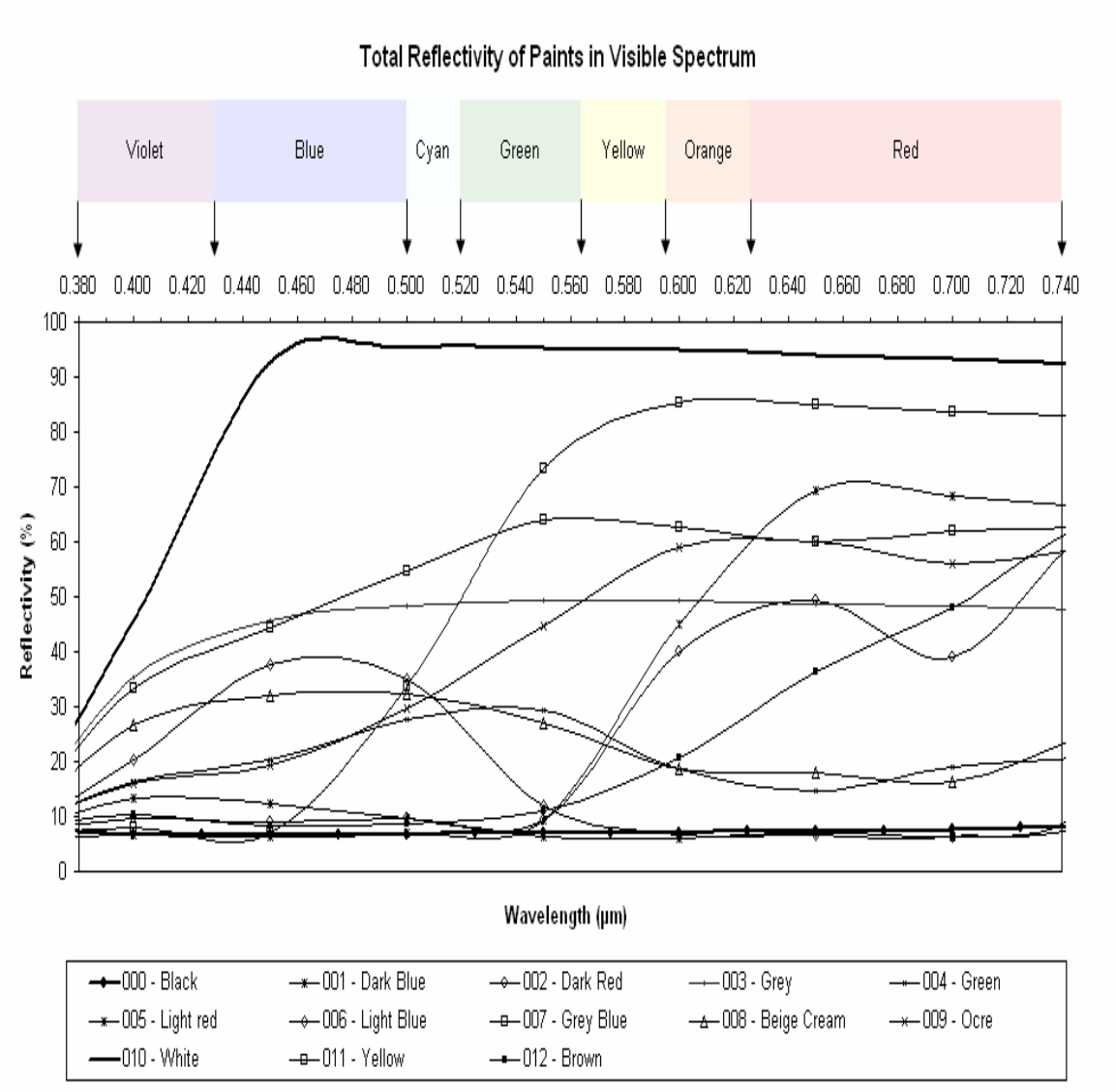

Figure 3 – Spectral reflectivity for paint samples in the visible spectrum

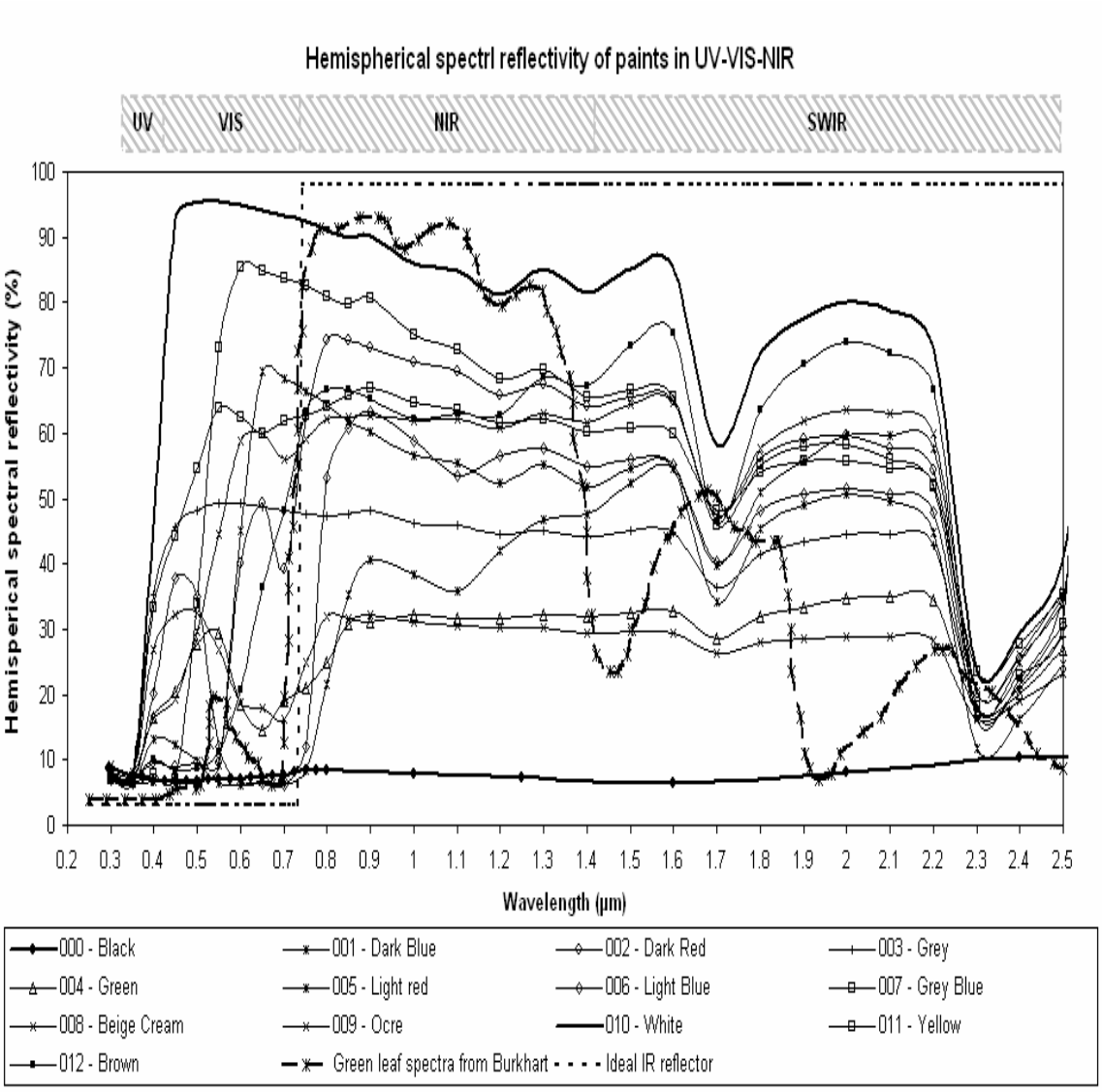

Figure 4 – Spectral reflectivity for the paint samples in UV-Visible and Near-IR spectrum

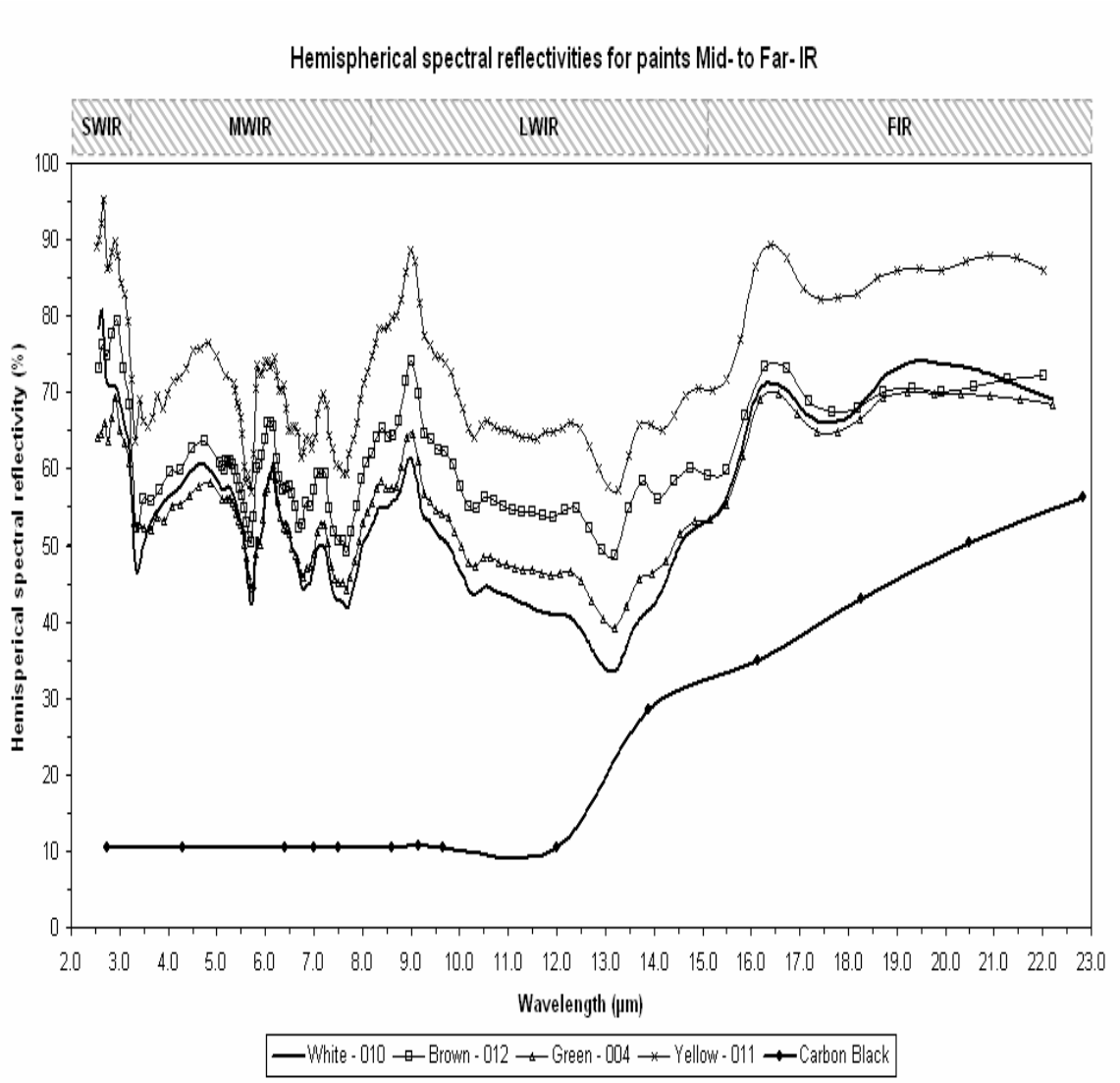

Figure 5 – Spectral reflectivity for the paint samples in the mid- to far IR spectrum

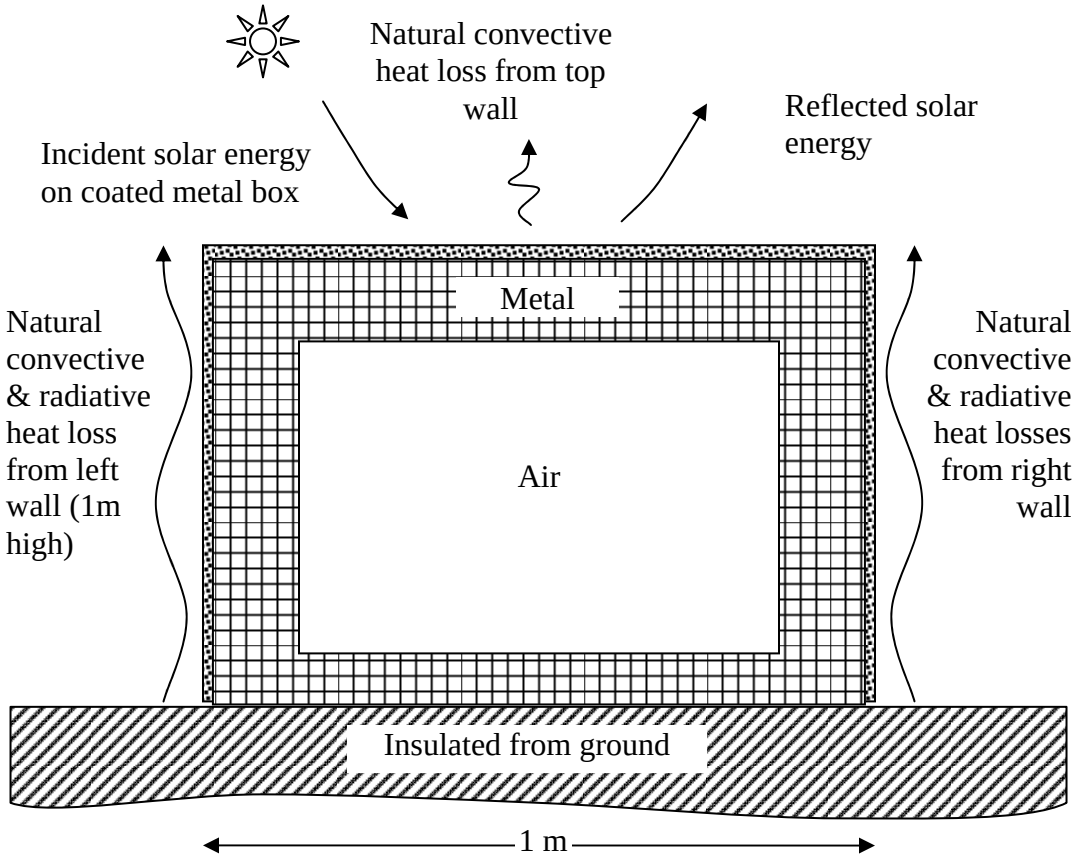

Figure 6 – Geometry of region of interest, metal walls are 6 mm thick and coating is 200μm

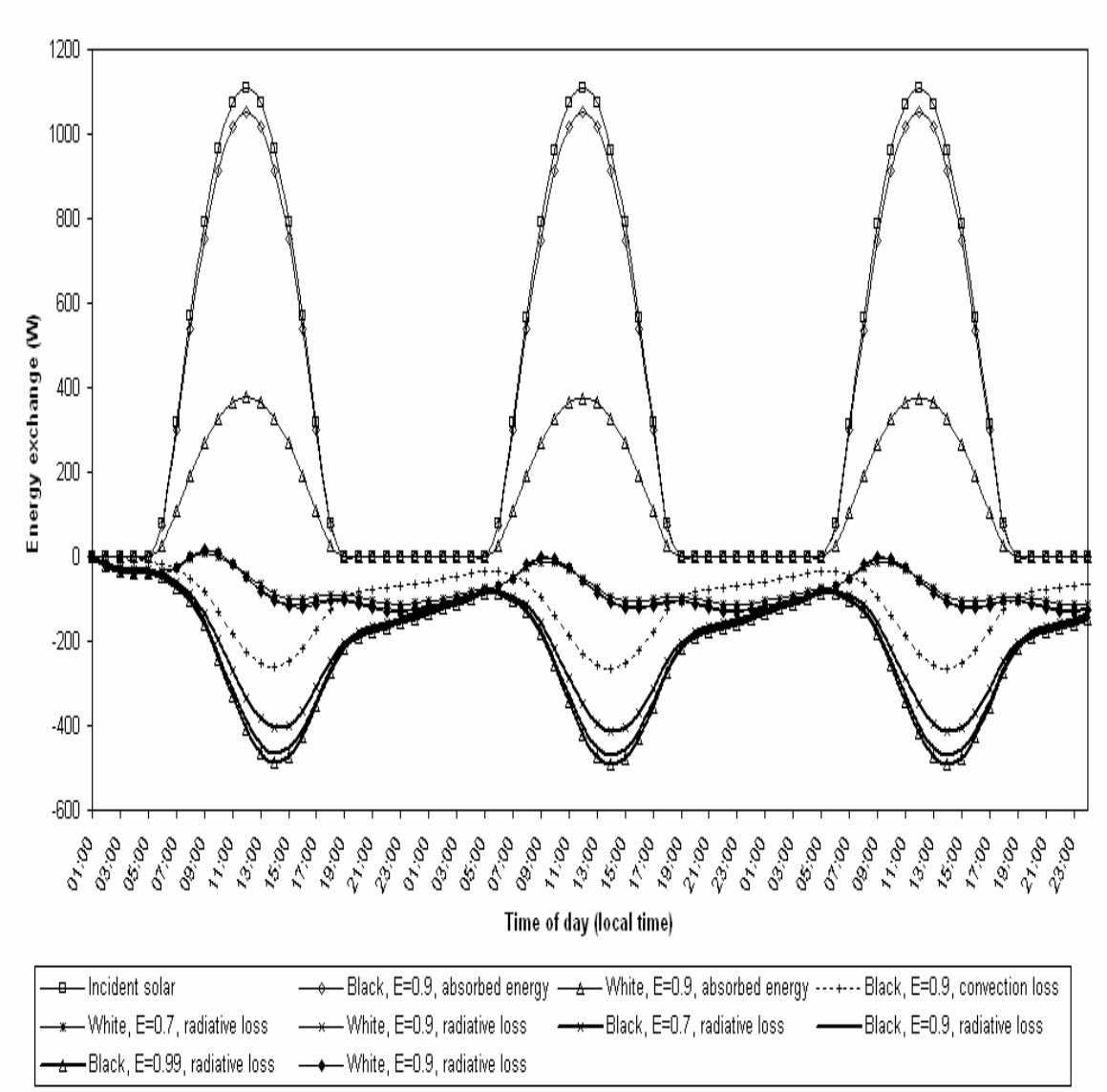

Figure 7 – Total incident and absorbed solar energy, together with convective and radiative heat loss in (W). The total emissivity ε_T used for radiative loss (referred to as E in graphs) is varied through 0.6 to 0.99.

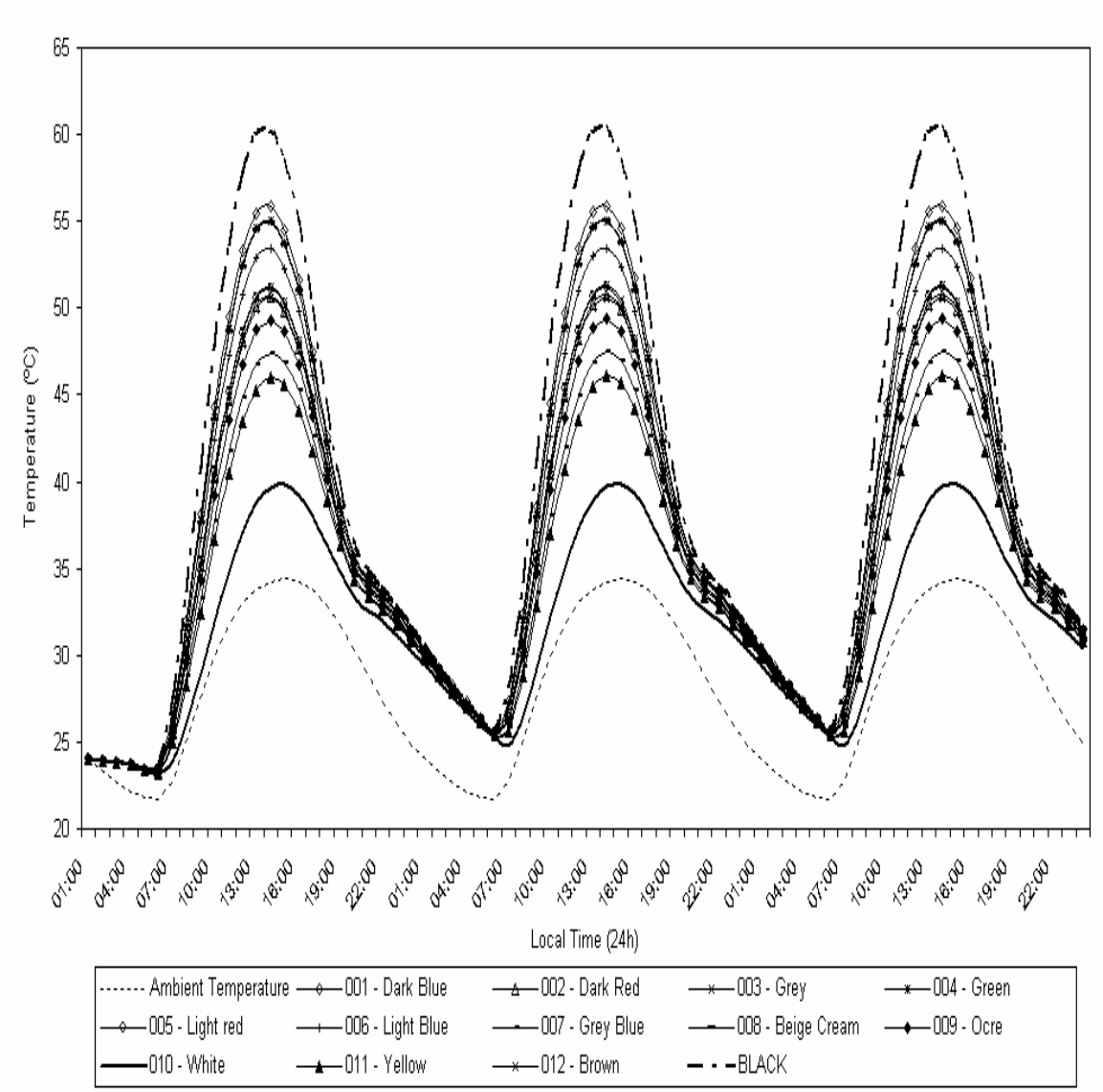

Figure 8 – Maximum diurnal temperatures for the metal with various paint coatings ranging from white to black.

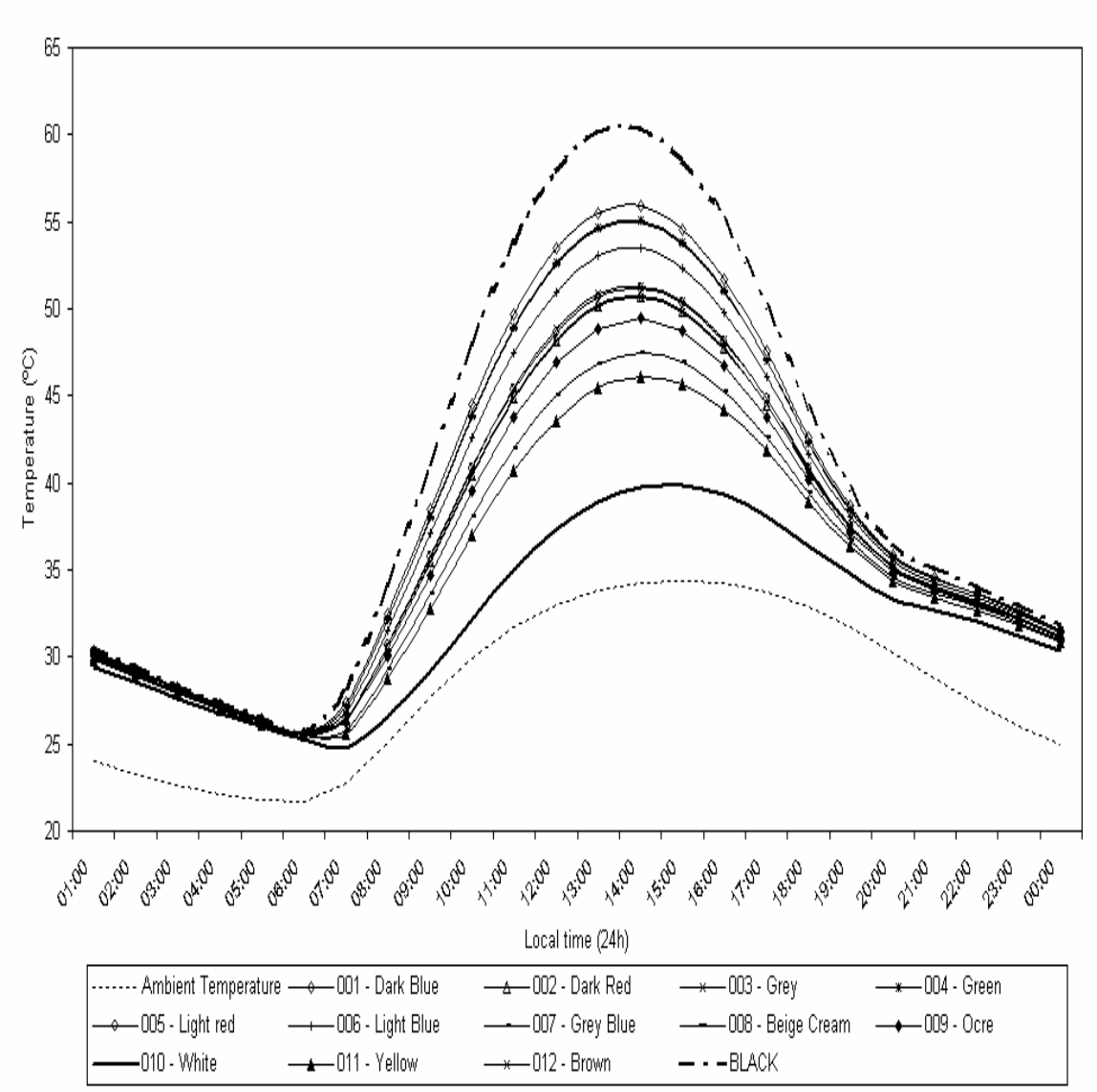

Figure 9 – 24 hour diurnal cycle of maximum temperatures of the metal/paint with all paints ranging from white to black

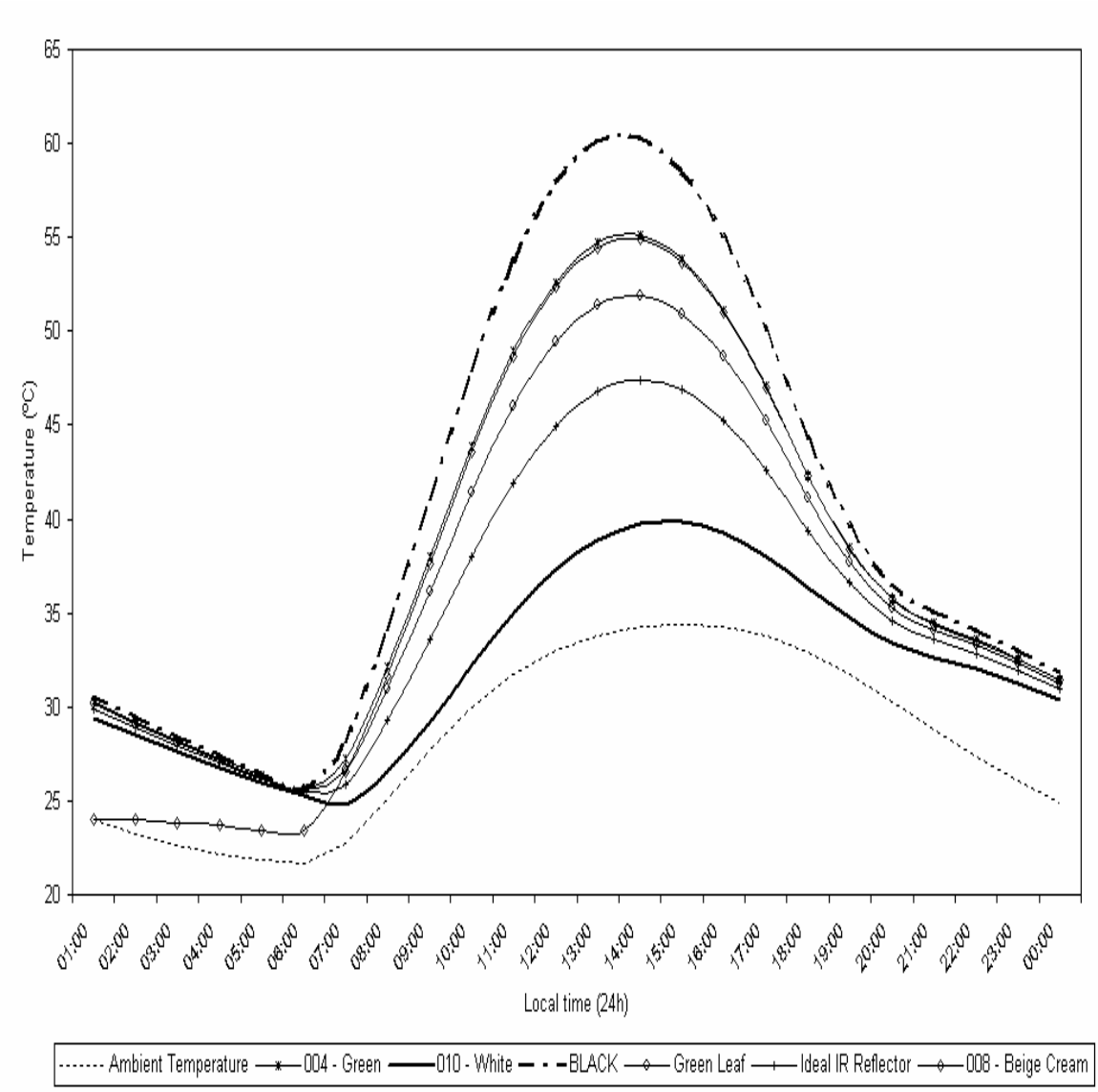

Figure 10 – 24 hour diurnal cycle of maximum temperatures of the metal/paint for selected paints (black, white, green) and compared to an ideal IR reflector and green leaf

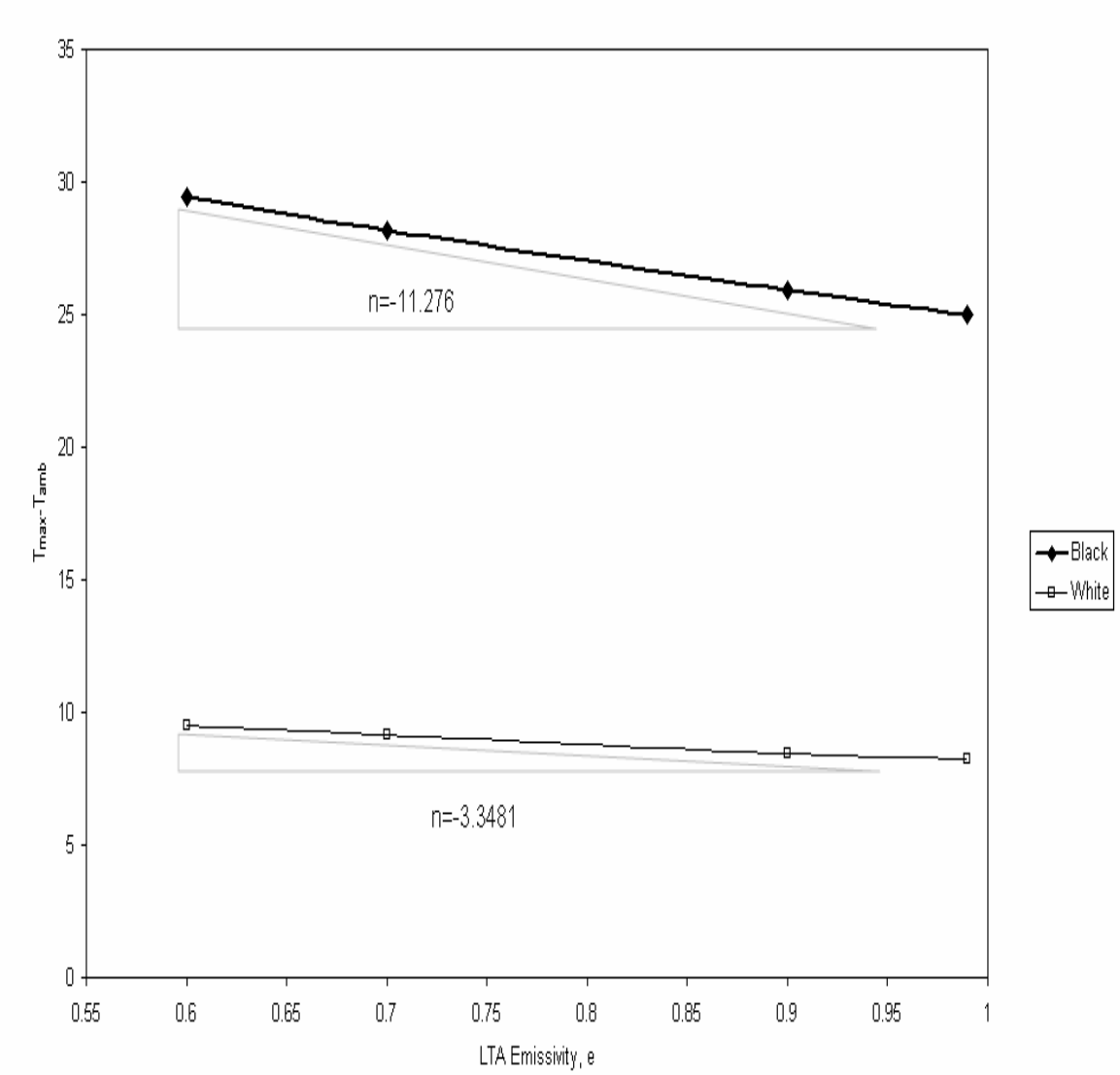

Figure 11 – Effect of the average low temperature emissivity on the surface temperature for black and white paints

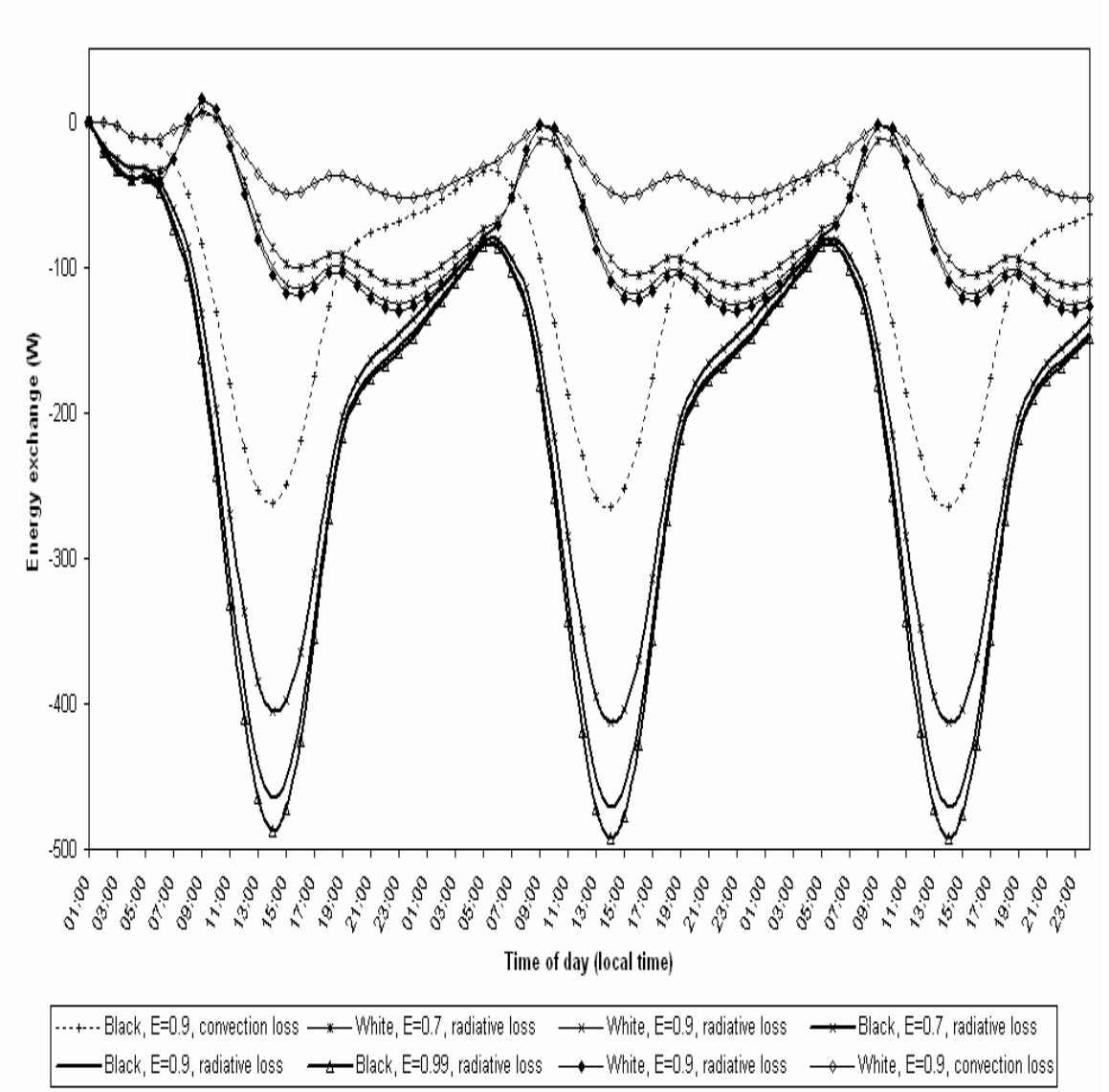

Figure 12 – Diurnal energy exchange in the body, in particular note the effect of the low temperature emissivity parameter on the radiative energy lost to the environment

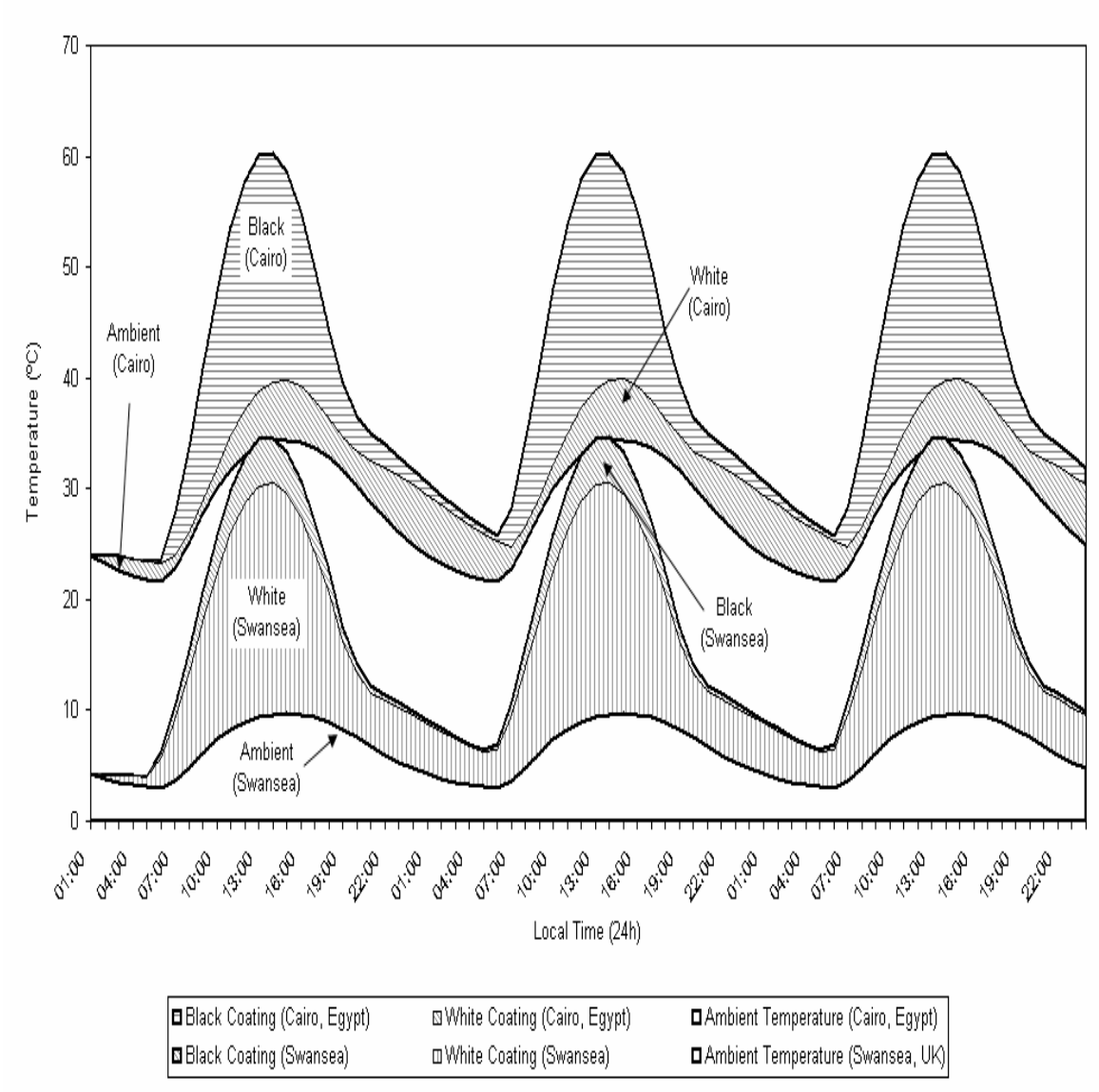

Figure 13 – Comparisons of maximum predicted diurnal temperatures for Cairo, Egypt compared to Swansea, UK